Defence Research and Development Canada
Recherche et développement pour la défense Canada

DEFENCE R&D DÉFENSE

Specification and Modelling of Maritime Surveillance and SAR Performance for Procurements

Michael K. McDonald and Anthony Damini

Defence R&D Canada – Ottawa
TECHNICAL REPORT
DRDC Ottawa TR 2004-238
November 2004

Canada

Specification and Modelling of Maritime Surveillance and SAR Performance for Procurements

Michael K. McDonald
DRDC Ottawa

Anthony Damini
DRDC Ottawa

Defence R&D Canada – Ottawa

Technical Report

DRDC Ottawa TR 2004-238

November 2004

Abstract

The work performed in support of the radar procurements for the Aurora Incremental Modernization Program (AIMP) and the Maritime Helicopter Program (MHP) during the evaluation and design phases is presented. The report focuses on the maritime surveillance and Synthetic Aperture Radar (SAR) modes and develops appropriate methods for predicting and modelling their respective performance. Issues such as the choice of appropriate target and clutter models, detection techniques and SAR imaging performance are described along with an analysis of the modelling limitations and cross-references to supporting documentation. The coupled issues surrounding the development of the requirements specification and the supporting test and verification plan are also discussed. The philosophies employed in the development of specifications and test plans, and the dependencies on the modelling limitations are presented and examples provided of how the requirements are tailored to complement the modelling techniques. A discussion of potential pitfalls in specification and testing approaches is provided along with examples.

Résumé

Le rapport présente les travaux menés à l'appui de l'acquisition de radars pour le Programme de modernisation progressive de l'Aurora (PMPA) et le Programme des hélicoptères maritimes (PHM) lors des phases d'évaluation et de conception. On y étudie les modes de surveillance maritime et SAR (radar à synthèse d'ouverture), et définit des méthodes de prédiction et de modélisation des performances respectives de ces deux modes. Le rapport s'intéresse entre autres au choix de modèles de cibles et de clutter, aux techniques de détection et à la performance de l'imagerie SAR, ainsi qu'à l'analyse des limites de la modélisation, et présente un système de renvois aux documents pertinents. La question de la spécification des exigences et de l'élaboration du plan connexe d'essais et de vérification est également abordée. Les principes d'élaboration des spécifications et des plans d'essai, et la dépendance de ces principes à l'égard des limites de modélisation, sont présentés, avec des exemples qui montrent comment les exigences sont définies de manière à compléter les techniques de modélisation. Le rapport examine les problèmes que peuvent poser les méthodes adoptées pour les spécifications et les essais, avec exemples à l'appui.

This page intentionally left blank.

Executive summary

This report documents work done over a multiyear period in support of the radar procurements for the Aurora Incremental Modernization Program (AIMP) and the Maritime Helicopter Program (MHP). The procurement of a radar is a complex task requiring multi-pronged evaluation and design phases in which issues such as functionality, maintenance, cost and performance are considered and balanced to achieve the optimal design solution. The work described in this report focuses on one aspect of this evaluation and design process, namely the specification and modelling of the maritime surveillance and Synthetic Aperture Radar (SAR) modes. The report summarizes the lessons learned during the procurement process and ties together a series of reports and memorandums developed in support of this project.

The report focuses on a broad range of issues that arise throughout the course of the procurement effort. Appropriate methods for predicting and modelling radar performance are developed and discussed along with an analysis of their limitations and cross-references to supporting documentation. Issues such as the choice of appropriate target and clutter models, detection techniques and SAR imaging performance are addressed in detail.

Having clearly established the limitations of our ability to model and characterize the radar performance, the coupled issues of preparing a requirements specification and a testing and verification plan are discussed. The philosophies employed in the development of the specification and test plans are highly dependent on the modelling limitations discussed above and examples are given of how the requirements are tailored to complement the modelling. Potential pitfalls in the development of specifications and test plans are identified and discussed with examples given.

McDonald, M.K. 2004. Specification and Modelling of Maritime Surveillance and SAR Performance for Procurements. DRDC Ottawa TR 2004-238. Defence R&D Canada - Ottawa.

Sommaire

Le rapport documente les travaux menés sur plusieurs années à l'appui de l'acquisition de radars pour le Programme de modernisation progressive de l'Aurora (PMPA) et le Programme des hélicoptères maritimes (PHM). L'acquisition d'un radar est une tâche complexe comportant des phases de conception et d'évaluation à multiples volets, lors desquelles des questions comme la fonctionnalité, la maintenance, les coûts et la performance sont étudiées et mises en perspective de manière à trouver la solution de conception optimale. Les travaux décrits dans le rapport visent essentiellement un aspect particulier de ce processus d'évaluation et de conception, soit la spécification et la modélisation des modes de surveillance maritime et SAR (radar à synthèse d'ouverture). Le rapport fait le point sur les connaissances acquises lors du processus d'acquisition et coordonne un ensemble de rapports et de mémoires rédigés dans le cadre de ce projet.

Le rapport examine un large éventail de questions qui se posent lors du déroulement du processus d'acquisition. Il définit et étudie des méthodes de détection et de modélisation de la performance du radar, et présente une analyse des limites de la modélisation, accompagnée de renvois aux documents pertinents. Des questions comme le choix de modèles de cibles et de clutter, les techniques de détection et la performance de l'imagerie SAR sont examinées en détail.

Après avoir nettement établi les limites de notre capacité de modélisation et de caractérisation de la performance du radar, le rapport aborde la question de la définition des spécifications d'un plan connexe d'essais et de vérification. Les principes d'élaboration des spécifications et des plans d'essai dépendent étroitement des limites de modélisation précitées; des exemples montrent comment les exigences sont définies de manière à compléter les techniques de modélisation. Le rapport identifie et étudie les problèmes que peut poser l'élaboration des spécifications et des plans d'essais, avec exemples à l'appui.

McDonald, M.K. 2004. Specification and Modelling of Maritime Surveillance and SAR Performance for Procurements. DRDC Ottawa TR 2004-238. R & D pour la défense Canada - Ottawa.

Table of contents

List of figures

List of tables

Acknowledgements

The authors express their thanks to the staff of PMO Aurora and PMO MHP as well as MacDonald Dettweiler and Associates for many useful discussions during the course of the radar procurements.

1. Introduction

This report documents work performed over a multiyear period in support of the radar procurements for the Aurora Incremental Modernization Program (AIMP) and the Maritime Helicopter Program (MHP). The procurement of a radar is a complex task requiring multi-pronged evaluation and design phases in which issues such as functionality, maintenance, cost and performance are considered and balanced when selecting the optimal design solution. The work described in this report focuses on one aspect of this evaluation process, namely the specification and modelling of the maritime surveillance and Synthetic Aperture Radar (SAR) modes. The report summarizes the lessons learned during the procurement process and ties together a series of reports and memorandums developed in support of this project.

The first part of the report focuses on the choice of appropriate models for sea clutter and target behaviour. The limitations of the available target and clutter models and the tractability of the detection performance solutions are discussed along with useful simplifications and approximations. Common detection schemes and algorithms are discussed along with their analysis and appropriate cross-references to supporting documentation.

In light of the limitations of the radar modelling, the coupled issues of preparing a requirements specification and a test and verification plan are discussed. The philosophies employed in the development of the specification and testing plans are highly dependent on the modelling limitations discussed above. Examples are given of how the requirements are tailored to complement the modelling.

The second section of the report deals with the performance of a surveillance radar operating in synthetic aperture modes. The conventional land imaging modes are stripmap or spotlight (landspot) SAR. The ocean-target imaging mode is seaspot SAR, which is a hybrid between SAR and Inverse SAR (ISAR).The system level performance of a SAR is looked at from three different viewpoints.

First of all, the dynamic range which the radar is capable of in its receive mode is discussed. Secondly, the actual imaging sensitivity of the radar is quantified. Finally, the imaging performance of the radar is summed up by examination of the output image quality through characterization of the impulse response of the radar. Dynamic range and radar sensitivity are derived from measurements and models. Impulse response characterization, or image quality, can be predicted by analysis or simulation but requires extensive modelling of the radar signal characteristics throughout the complete transmit, receive and

processing chains. Therefore, we discuss impulse response characterization in a more straightforward manner, through measurements on real images containing known corner reflectors.

2. Radar Detection Performance

2.1 Radar Target Models

The use of target models greatly simplifies the task of evaluating radar performance although the idealized models may fail to capture some of the characteristics of the actual targets to be encountered. For the purposes of the procurements discussed in this report we have adopted the use of the Swerling target models and developed the corresponding detection theory. The Swerling targets have the advantage of being well known and mathematically tractable.

The Probability Density Function (PDF) corresponding to the Swerling models is given as

$$p(R) = \frac{k^k}{\Gamma(k)\,\bar{R}^k} R^{k-1} \exp\left(\frac{-kR}{\bar{R}}\right) \tag{1}$$

where $\bar{R}$ is the average signal power and k=1,N,2,2N corresponds to the Swerling classes I, II, III and IV, respectively [1]. While the Swerling models may not always represent the most accurate model for describing some real life targets, they are nevertheless extremely useful for quantitative comparisons of different radars as well as an excellent model for cooperative targets that might be deployed during field trial testing.

The different Swerling models are tailored to represent four broad classes of received target signals. Swerling 1 and 2 target models correspond to complex targets comprised of a large number of independent scatters of similar scattering cross-section i.e. no scatterer is dominant. Swerling case 1 and 2 differ in regards to the rate at which the frequency fluctuations are assumed to occur. Swerling 1 target amplitudes are assumed to remain constant over short periods of time, typically taken as the period of time the target remains within the antenna beamwidth during a single scan. Target fluctuations are assumed to occur on a scan to scan basis. The assumption underlying this model is that the geometric, and therefore phase relationship, between the radar receiver and the target change very little during this short time period. While this condition may be maintained for a radar employing a constant centre frequency, it is unlikely to be met for frequency agile radars which transmit successive pulses at different centre frequencies. For this case the Swerling 2 target model is more applicable as it allows the cross-section to vary from pulse to pulse. This model has been assumed for small targets, such as periscopes and speed boats,

that are identified in the requirements specification. The choice of target model is discussed in more detail in later sections of the report.

Swerling cases 3 and 4 assume that fluctuations occur on a scan to scan and pulse to pulse basis, respectively, but in this case there is assumed to be one dominant scatterer with a much larger cross-section then the numerous scatterers surrounding it. The target return power is dominated by the strength of the reflection from this primary scatterer with small fluctuations induced by the interference effects of the smaller scatterers. The latter models can be applicable to such maritime targets as tankers or military ships. For the case of a dominant scatterer, the Swerling 3 and 4 models are useful approximations, while a more precise model is the Rice distribution. The Rice PDF is given by

$$p(R) = \frac{1+s}{\bar{R}} \exp\left[-s - \frac{R}{\bar{R}}(1+s) \right] I_o\left(2\sqrt{\frac{R}{\bar{R}} s(1+s)} \right) \qquad (2)$$

where s is the ratio of the dominant scatterer cross section to the total of the secondary scatterer's cross section [1]. Despite its direct relationship to a physical scattering model, the Rice distribution was not used in the MHP and AIMP procurements due the greater mathematical complexity of its application in comparison with Swerling models. In addition, the use of the Swerling models is typically sufficient to highlight the differences between competing radars and to draw out the performance characteristics for each radar. The greater familiarity of radar manufacturers with the Swerling models also reduces the effort required by a manufacturer to produce a bid and tends to lead to more detailed responses.

2.2 Modelling Sea Clutter

2.2.1 Stochastic Models for Clutter

The study of radar detection in clutter has traditionally relied on the application of stochastic theory to evaluate target detection schemes. In theory, modelling sea clutter with an appropriate statistical distribution allows the calculation of the detection probability for a specified false alarm rate. Early studies of sea clutter returns from low resolution radars were quite successful in applying the Gaussian probability distribution to the detection problem; the success of this approach made intuitive sense as the total return from any resolution cell (nominally the area defined by the beamwidth and range resolution of the radar) could be viewed as the sum of the many scatterers within it; for a very large numbers of scatterers the application of the central limit theorem (CLT) will result in the aforementioned Gaussian distribution. The theory

surrounding the application of the Gaussian distribution is well developed, Skolnik [1], for example, provides a good introduction.

Since the strength of clutter returns is directly proportional to the cell area being viewed, it was anticipated that improving the range resolution of radars systems (i.e. smaller resolution cell areas) would result in a corresponding improvement in detection capability. Unfortunately, this did not prove necessarily true as an increasingly impulsive or spiky character was observed to develop in the clutter returns as the cell size was decreased. The observed breakdown of the Gaussian behaviour is the result of bunching of scatters due to correlations in the underlying sea surface structure. To overcome the aforementioned shortcomings, several other distributions have been suggested as models for the statistics of sea clutter returns, the most common being the log-normal, Weibull and K-distribution.

In recent years the K distribution has become the most prominent choice due to its success in approximately a broad range of clutter conditions. The K distribution also offers the assurance of corresponding to a realistic physical model. The K distribution presumes that overall return, *x*, is composed of a speckle component *p(x|y)* with a mean power, *y*, modulated per the underlying texture distribution *p(y)*,

$$p(x) = \int_{all\ y} p(y)\, p(x \mid y) dy \tag{3}$$

[2,3,4]. The speckle component is well modelled by a Rayleigh distribution,

$$p(x \mid y) = \frac{2x}{y} \exp\left(\frac{-x^2}{y} \right), \tag{4}$$

while the texture distribution is typically found to be a good fit to the gamma distribution

$$p(y) = \frac{c^{2\nu} y^{\nu-1}}{\Gamma(\nu)} \exp(-c^2 y), \tag{5}$$

where ν is the shape parameter and *c* is the scaling factor. The textural component can be visualized as arising due to the gross structure of the sea surface swell while the speckle arises from the more complicated and smaller scale capillary wave structure. It is observed that the speckle component of clutter possesses very short correlation times on the order of milliseconds while the texture component remains correlated over time scales on the order of seconds. Similarly it is observed that while speckle components will rapidly

decorrelate if the clutter patch under observation is shifted any distance, the textural spatial correlation is on the order of 10 meters. The impact of these different scales of decorrelation and some methods of dealing with them during modelling is discussed in the following sections.

For the reasons discussed above, the K distribution was adopted as the best description of the PDF of the sea clutter returns for these procurements. It is used throughout the rest of the report and forms the basis on which the detection performance prediction algorithms are based. Unfortunately, the K distribution proves less tractable in comparison with the Gaussian distribution often necessitating the use of numerical methods to model the performance; this aspect is discussed in more detail in the following sections.

It should be noted that the simple Rayleigh model for sea clutter is a subclass of the overall K-distribution corresponding to the case where the shape parameter of the gamma distribution approaches infinity. Practically the PDF will appear quite Rayleigh-like for shape parameters as small as 10 and under these conditions the simpler Rayleigh distribution can often be used without noticeable impact on the performance predictions.

2.2.2 Clutter Parameters

The key parameters that must be determined in support of radar performance modelling of the clutter are the clutter cross section and shape parameter. To date, the complex and variable nature of sea surface dynamics has precluded the development of a reliable analytic predictor of cross section and shape parameter. Therefore, the models that are employed have been empirically derived from data bases of sea clutter returns.

The upshot of this is that it is not possible to definitively choose a ‘best’ clutter model. Different manufacturers and countries will often use different models depending on the database of measurements they have at their disposal. Since all are based on empirical measurements, they are all are ‘correct’, any differences between the derived models represents shortcomings in the fidelity of the individual models i.e. the model details and parameters are insufficient to capture all the potential scenarios.

For the work described herein, the clutter cross-sections have been calculated using the Georgia Institute of Technology (GIT) clutter cross-section model [5]. The GIT model has the benefit of being widely used and most radar manufacturers will have a familiarity with its use. The GIT outputs the mean clutter reflectivity associated with a given sea state, look direction with respect to the wind, polarization, grazing angle and radar wavelength.

The GIT has some significant limitation which must be kept in mind during its' use. If all parameters are within the bounds for which the GIT model was designed there is still an approximate 5 dB one sigma variation in the clutter cross-sections from the model prediction [5]. Equally important is the inability of the model to capture the difference in clutter cross-sections between upwind and downwind viewing directions. It is easily observed on real radar displays that the upwind viewing direction frequently produces stronger clutter returns then the downwind direction. This difference arises due to the enhanced reflection of incident energy from the curved wave front on the sea surface. While the GIT clutter model does incorporate a viewing direction dependence it is symmetric across the axis between upwind and downwind directions. Consideration of these effects is likely to be particularly important during the analysis of field trial results. A deeper discussion of field trial issues is included in latter sections of the report.

The shape parameter used in the modelling has been determined using the empirical relationship derived by Watts et al [6,7], namely

$$\log_{10}(\nu) = \frac{2}{3}\log_{10}(\varphi) + \frac{5}{8}\log_{10}(L_c) + \frac{5}{8}\log_{10}\left(\frac{\Delta R}{4}\right) - \frac{1}{3}\cos(2\theta_{SW}) - 1, \qquad (6)$$

where

φ =the grazing angle (deg),

L_c is the cross range resolution given by $\Delta\theta * R_g$,

θ_{SW} is the angle between the boresight and the swell direction (zero when boresight is pointed in swell direction).

The most important point to keep in mind from a procurement point of view is that all parties agree on a common model to use. In many cases its is the relative differences between radars which are most pertinent, even in cases where only one radar is being modelled it is important to ensure that all parties are working with the same assumptions.

Table 1: Models used for AIMP and MHP procurements evaluations.

Parameter	Model Used
Radar Target	Swerling 2 and 4 [1]
Clutter PDF	K-distribution [2,3,4]
Clutter Cross-section	GIT clutter cross-section model [5]
Clutter Shape Parameter	Watts et al. empirical formula [6,7]

2.3 Modelling Radar Detection Performance

2.3.1 Single Pulse Versus Integrated Detection

The simplest type of measurement to analyse is the single pulse. The corresponding equation for the Probability of False Alarm (PFA) is well known and given by

$$PFA_{single\ pulse} = \exp\left(-\frac{T}{2y}\right) \tag{7}$$

where T is the threshold for declaring a detection and y is the underlying clutter power which would need to be estimated in a practical detection scheme [1]. It should be emphasized that while y remains constant for Rayleigh clutter (at least in a local sense) it will vary with both location and time for K-distributed clutter.

There are two general ways of applying a detection threshold; a fixed threshold or a varying threshold. Fixed threshold detection occurs when incoming measurements are compared against a threshold value that remains constant across all measurements to determine if a detection occurs. Fixed threshold detection is simple but non-optimal in most cases as it cannot adjust to the underlying variation in the texture (average power) of the clutter returns, it also requires that a global measure of the overall clutter power level be available i.e. y_{avg}. The green line in figure 1 illustrates the effect of using a fixed threshold to achieve a specified PFA. It can be seen that those regions in which larger peaks occur primarily dictate the setting of the threshold. Note that an estimate of global clutter power (i.e. over a large region) is still required to accurately set the fixed threshold.

In contrast, a varying threshold is set according to an estimate of the underlying clutter power obtained from the local region of the range return that is currently under test. The red line in figure 1 shows the threshold required at each point to obtain an identical PFA result when the underlying texture is perfectly known. It can be seen that the varying threshold more closely follows the underlying power fluctuations and will allow for more efficient detection of targets in regions with low clutter power.

Real radar systems typically employ a variety of methods to estimate the underlying background power. The best documented approach is the Cell Averaging Constant False Alarm Rate (CA-CFAR) [see for instance 8] in which a sample of background cells surrounding the Cell Under Test (CUT) are averaged to form a background estimate. Depending on the size of the background block and the correlation length of the texture of the sea clutter, this technique produces either a local or global estimate. By local it is meant that the estimate reflects the underlying clutter power in the CUT; mathematically this corresponds to a given value in the texture. The global estimate represents the average clutter power over a large region; mathematically this corresponds to the mean of the PDF representing the texture. Of course neither of these estimates is perfect and estimates will typically fall within these two extremes depending on the ratio of the correlation length of the clutter to the background length.

While simple, the single pulse equation above is not usually of much interest as it is typically necessary to integrate multiple measurements to improve the signal to noise ratio (SNR) and achieve reasonable detection performance against small targets. For the purpose of the procurements discussed above all integration was applied post-envelope detection, i.e. the phase information was lost. Several different methods of integration were considered in this work; in order of increasing complexity the integration methods considered in this report are binary integration, non-coherent integration and peak detection.

It is common for a processing chain to make use of more then one type of integration. A typical example is the use of pulse to pulse non-coherent integration during the antenna dwell (i.e. the time it takes the antenna to sweep across a target) followed by binary integration on a scan to scan basis. Because of the short time span between the pulses integrated within the dwell (pulse repetition frequencies are typically on the order of a few hundred Hz or higher) the underlying texture of the clutter can be assumed to remain fully correlated over the dwell. To ensure that the speckle component, which typically has correlation times on the order of ms, fully decorrelates from pulse to pulse it is common for radar systems employing pulse to pulse integration to also use a frequency agile transmission pattern in which the centre frequencies of the

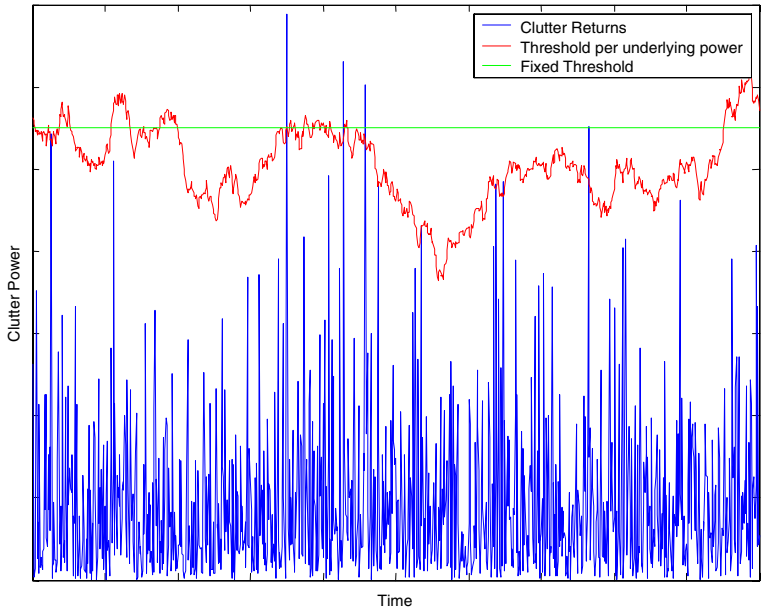

Figure 1. Fixed and variable threshold settings to achieve equivalent PFA.

contiguous pulses are shifted so that that bandwidths do not overlap. This technique is very effective in decorrelating the clutter and in the subsequent theoretical development the speckle is assumed to be fully decorrelated between pulses.

2.3.2 Detection Performance of K-distributed Clutter with Temporally Correlated Texture

Hou and Morinaga [9] formulated the detection performance of different Swerling targets in K-distributed clutter against a fixed threshold. Their derivation assumed that the texture of the integrated pulses remained fully correlated while the speckle component fully decorrelated. This situation most closely corresponds to the case where pulse to pulse non-coherent integration with frequency agility is applied.

Per Hou and Morinaga the characteristic function corresponding to the PDF of the single pulse Rayleigh distributed square law detected envelop is given as

$$C(z \mid y,S) = \frac{e^{\frac{-Sz}{2(1+zy)}}}{(1+zy)} \tag{8}$$

where S is the signal power and the variations in underlying texture or power distribution, y, is retained. The N pulse integrated solution is found simply by raising the single pulse characteristic to the power N, i.e.

$$C(z \mid y,S,N) = \frac{e^{\frac{-NSz}{2(1+zy)}}}{(1+zy)^N} \tag{9}$$

If the target power is fluctuating it is necessary to integrate the characteristic over the corresponding target PDF, $p(R)$.

$$C_{fluctuating}(z \mid y,S,N) = \int_{all\ R} p(R) \frac{e^{\frac{-NSz}{2(1+zy)}}}{(1+zy)^N} dR \tag{10}$$

The PDF corresponding to the Swerling models was given above as

$$p(R) = \frac{k^k}{\Gamma(k)\bar{R}^k} R^{k-1} \exp\left(\frac{-kR}{\bar{R}}\right) \tag{11}$$

where $\bar{R}$ is the average signal power and k=1,N,2,2N corresponds to the Swerling classes I, II, III and IV, respectively. The resulting characteristic function for the Swerling target model is then

$$C_{fluctuating}(z \mid y,S,N,k) = \frac{(1+zy)^{k-N}}{\left[1+z\left(y+\frac{N\bar{S}}{2k}\right)\right]^k} \tag{12}$$

The corresponding y dependent $PFA_{fixed\ threshold}(y,0,N,k)$ and $PD_{fixed\ threshold}(y,S,N,k)$ for a given threshold T, can be derived using the residue theorem giving

$$
\begin{aligned}
&\int_T^\infty p(x \mid H_{0,1})\, dx \\
&= \int_T^\infty \sum_k res[C_{fluctuating}(z \mid y,S,N,k)e^{zx}, z_k]\, dx \\
&= -\sum_k res\left[C_{fluctuating}(z \mid y,S,N,k)\frac{e^{Tz}}{z}, z_k\right] \\
&= -\sum_{k_0} \frac{1}{(m-1)!} \lim_{z \to z_k} \sum_{n=0}^{m-1} \binom{m-1}{n} \frac{\partial^{m-1-n}}{\partial z^{m-1-n}} \left((z-z_k)^m C_{fluctuating}(z \mid y,S,N,k)\right) \frac{\partial^n}{\partial z^n} \int_T^\infty e^{zx}\, dx \\
&= -\sum_{k_0} \frac{1}{(m-1)!} \lim_{z \to z_k} \sum_{n=0}^{m-1} \binom{m-1}{n} \frac{\partial^{m-1-n}}{\partial z^{m-1-n}} \left((z-z_k)^m C_{fluctuating}(z \mid y,S,N,k)\right) \frac{\partial^n}{\partial z^n} \frac{e^{zT}}{z}
\end{aligned}
\tag{13}
$$

where z_k is the mth order pole and H_0 and H_1 correspond to the target absent and present cases respectively. The above fixed threshold result derived by Hou and Morianaga must then be integrated across the appropriate texture distribution. For the K-distribution the underlying texture PDF is gamma distributed and given by

$$
p(y) = \frac{c^{2\nu} y^{\nu-1} e^{-c^2 y}}{\Gamma(\nu)} \tag{14}
$$

where ν is the shape parameter and c is a scaling parameter. The average power, $E(y)$, is related to the shape parameter and scaling parameter per $E(y) = \frac{\nu}{c^2}$. The resulting expression for $PFA_{fixed\ threshold}(0,N,k)$ and $PD_{fixed\ threshold}(S,N,k)$ is then

$$
\int_0^\infty p(y) \left(-\sum_{k_0} \frac{1}{(m-1)!} \lim_{z \to z_k} \sum_{n=0}^{m-1} \binom{m-1}{n} \frac{\partial^{m-1-n}}{\partial z^{m-1-n}} \left((z-z_k)^m C_{fluctuating}(z \mid y,S,N,k)\right) \frac{\partial^n}{\partial z^n} \frac{e^{zT}}{z} \right) dy \tag{15}
$$

where the integration is performed numerically.

As discussed above the fixed threshold formulation of Hou and Morianaga is limited in its usefulness as it does not predict performance of varying threshold detection schemes and more particularly, CA-CFAR.

The approach above can be extended to include the CA-CFAR approach by modifying the lower limit, T, of the integration in line 4 of equation 13. The fixed threshold value T is replaced by a varying limit given by αy_e where y_e is

the estimate of the background power and α is the threshold multiplier chosen to achieve the specified PFA. For this formulation the texture, *y*, is assumed constant across all the cells included in the background measurement, with each cell comprising a *y* dependent Rayleigh variable. Summing over the *M* background cells and across *N* integrated scans gives $L = M * N$ individual samples and the corresponding y_e PDF

$$p(y_e \mid L, y) = \frac{\left(\frac{1}{y}\right)^L y_e^{L-1} e^{\left(\frac{-y_e}{y}\right)}}{(L-1)!} \tag{16}$$

Integrating across all possible values of y_e gives

$$\begin{aligned} &PD_{CA-CFAR}(y, S, N, k) \\ &= -\sum_{k_0} \frac{1}{(m-1)!} \lim_{z \to z_k} \sum_{n=0}^{m-1} \binom{m-1}{n} \frac{\partial^{m-1-n}}{\partial z^{m-1-n}} \left((z - z_k)^m C_{fluctuating}(z \mid y, S, N, k) \right) \frac{\partial^n}{\partial z^n} \int_0^\infty e^{z x y_e} f(y_e) dy_e \\ &= -\sum_{k_0} \frac{1}{(m-1)!} \lim_{z \to z_k} \sum_{n=0}^{m-1} \binom{m-1}{n} \frac{\partial^{m-1-n}}{\partial z^{m-1-n}} \left((z - z_k)^m C_{fluctuating}(z \mid y, S, N, k) \right) \frac{\partial^n}{\partial z^n} \frac{1}{z\left(\frac{1}{y} - \alpha z\right)^L} \end{aligned} \tag{17}$$

The final result for a K-distribution is again obtained by integrating across all values of *y* per the PDF given in equation 14. For the case of $PD_{CA\text{-}CFAR}(S,N,k)$ the integration is performed numerically. For $PFA_{CA\text{-}CFAR}$ the dependency on *y* vanishes leaving the simplified formula

$$PFA_{CA-CFAR}(0, N, k) = \sum_{m=0}^{N-1} \binom{L+m-1}{L-1} \frac{\alpha^m}{(1+\alpha)^{L+m}} \tag{18}$$

The expression is applicable to both Rayleigh and K-distributed clutter in which the texture remains constant across the background and CUT for all integrated pulses.

Another useful approximation that can reduce the required processing time is to use the expression given by Oliver [10] for integrated clutter where the underlying texture is assumed to be constant across *N* pulses but varying per the gamma distribution over longer time scales. The expression is given as

$$p(I) = \frac{2}{I}\left(\frac{N\nu I}{\langle I \rangle}\right)^{\frac{N+\nu}{2}} \frac{1}{\Gamma(N)\Gamma(\nu)} K_{\nu-N}\left[2\left(\frac{N\nu I}{\langle I \rangle}\right)^{\frac{1}{2}}\right] \tag{19}$$

where I is the intensity and $\langle I \rangle$ is the average power. For the case where the underlying power remains constant the intensity is given by the simple gamma distribution of equation 14 above, or written in terms of the parameter I it is given as

$$p(I) = \frac{1}{I}(NI)^N \frac{1}{\Gamma(N)} \exp(LI) \tag{20}$$

The above equations are easily evaluated over a broad range of values and a piecewise integration can be performed to determine the threshold required to produce a given PFA. To determine the PD for the case where a Swerling 2 target is assumed present it is possible to employ another approximation. If it is assumed that the PDF of the target plus clutter is primarily gamma (or equivalently chi squared) in nature, i.e. the Swerling 2 target characteristics dominate, then the PD can be calculated in a similar piecewise fashion to the PFA above using the combined PDF given by

$$p(I) = \frac{1}{I}\left(\frac{NI}{S+1}\right)^N \frac{1}{\Gamma(N)} \exp\left(\frac{LI}{S+1}\right) \tag{21}$$

where S is the signal to clutter plus noise ratio. This approximation has been shown to give very good results for shape parameters within the range of interest.

2.3.3 Binary Detection

Binary integration is a well-documented integration technique [see for example 11] utilizing a dual threshold. Each measurement is compared against a decision threshold, if the threshold is exceeded a binary one is assigned to the results and a zero if the threshold is not exceeded. The binary outcomes from N measurements are summed and compared against the secondary threshold, M. If the M out of N decision threshold is met or exceeded a target is declared to be present.

In practical systems, binary detection is typically applied on a scan to scan basis. For the case where scan rates are low (i.e. on the order of seconds between scan to scan measurements) the individual measurements can often be safely assumed to be fully independent (texture fully decorrelates) and the overall PFA and PD calculated via the simple combinational relationship

$$PFA_{binary}(0,N,k) = \sum_{k=M}^{N} \binom{N}{k} \left[PFA_x(0,1,k)\right]^k \left[1 - PFA_x(0,1,k)\right]^{N-k} \tag{22}$$

$$PD_{binary}(S,N,k) = \sum_{k=M}^{N} \binom{N}{k} \left[PD(S,1,k)\right]^{k} \left[1 - PD_{x}(S,1,k)\right]^{N-k} \tag{23}$$

where the subscript *x* corresponds to either *fixed threshold* or *CA-CFAR*.

The other extreme corresponds to the case where the texture remains fully correlated across scans. This scenario is less likely to occur, as it requires a very fast scan rate with a long texture correlation time. In this case the individual probabilities measurements within the combinational are the *y* dependent probabilities of equations 13, 17 or 18 as applicable. The numerical integration over the texture *y* is moved outside the combinational operator i.e.

$$PFA_{binary}(0,N,k) = \int_{0}^{\infty} p(y) \sum_{k=M}^{N} \binom{N}{k} \left[PFA_{x}(y,0,1,k)\right]^{k} \left[1 - PFA_{x}(y,0,1,k)\right]^{N-k} \partial y \tag{24}$$

$$PD_{binary}(S,N,k) = \int_{0}^{\infty} p(y) \sum_{k=M}^{N} \binom{N}{k} \left[PD(y,S,1,k)\right]^{k} \left[1 - PD_{x}(y,S,1,k)\right]^{N-k} \partial y \tag{25}$$

The intermediate case occurs when the texture is partially correlated across scans making up an integration set. Currently the closed form solution of this problem is not mathematically tractable although Monte Carlo methods have been applied to address the problem [12]. Unfortunately the application of Monte Carlo methods requires that the correlation be specified prior to Monte Carlo simulation. When correlation times are unknown a priori, or a large range of different lengths are encountered it becomes impractical to generate results to cover all conditions. Under these conditions it is common to characterize the loss factors for a chosen set of temporal correlation lengths spanning the range of values that are expected under real conditions. This set of loss factors is then used to calculate loss factors for other temporal correlations by interpolating between the values.

2.3.4 Non-Coherent Integration

While non-coherent integration with constant texture has already been treated in the proceeding discussion, in most practical detection scenarios the constant texture condition will not be met across the full scan to scan integration period where integration periods of 5 seconds or more are typically required to acquire sufficiently large detection probabilities. This significantly complicates the analysis.

At one extreme lie radars scanning at rates of several hundred rpm. For these radars pulse to pulse integration techniques are typically not employed as the target only remains within the antenna dwell for one or two pulses. If the temporal length of the texture correlation coefficient is very short it can often be assumed that the texture completely decorrelates between scans. In this case the PDF expressions for each scan reduce to the single measurements results; the effect of integrating several scans can then be determined by numerically convolving the single measurement PDFs.

The intermediate case where the texture is partially correlated between pulses proves the most difficult to handle. Monte Carlo methods can again be brought to bear on the problem but they suffer from the same limitation as binary integration in that it is difficult to vary the imposed correlation.

Another useful technique, which can help to place limits on the expected performance under partial correlation, is to divide the integration set into subsets corresponding to the texture correlation length. As a worst case scenario, each a subset is assumed to correspond to a single measurement so that the total number of integrated measurements is equal to the number of subsets. The single scan expressions of equations 19 through 21 are then numerically convolved over the number of subsets. This worst case estimate provides one limit on the anticipated performance. A best case estimate, in which all measurements are assumed to be completely independent and the appropriate equation is numerically convolved over all measurements, provides the other limit. Figure 2 illustrates one example for the case in which 15 measurements are integrated with a textural correlation corresponding to 5 measurements. Despite the fact that there is a 5:1 ratio between the number of independent measurements assumed for each case there is at worst a 3 dB difference in the target cross-section required to achieve a 50% probability of detection. The actual performance will lie somewhere in between. Performing Monte Carlo simulations for selected conditions and using the results as a guide for interpolating between the curves can further refine rough estimates of where the actual performance lies.

2.3.5 Peak Detection

Peak detection is a selection process designed to reduce the bandwidth of the incoming signal, i.e. reduce the number of range cells for further processing. Peak detection works by subdividing the full range of measured microcell values into macrocells. The maximum valued microcell within a given macrocell is then chosen to represent the power of the coarser resolution macrocell, see figure 3. Most modern radar systems do not utilize bandwidth reduction techniques prior to detection in their primary channels as this results in collapsing losses which degrade the detection performance. However, it is

common to paint the display screen with an underlay reflecting the 'raw' data returns. Given that a high resolution radar could be returning measurements at a range spacing of less than 0.5 meters over tens of nautical miles, there is a significant mismatch with respect to the resolution of the display screens which can typically display on the order of a thousand pixels in any direction. The underlay display is important as it can be viewed as a secondary detection channel on which the radar operator will be able to distinguish targets (or equally important, eliminate false targets) by visual inspection. The need to employ bandwidth reduction techniques introduces a collapsing loss which degrades the operator's ability to detect a target.

Peak detection is the most common way in which this bandwidth reduction is achieved. Under simple clutter conditions of Rayleigh distributed clutter, the PDF of the peak detected value of *n* samples is easily derived from the ordered statistics PDF [13] as

$$p_n(x) = nF^{n-1}(x)\,p(x)\,dx \tag{26}$$

where

$$p(x) = \frac{1}{P_{avg}} e^{-\frac{x}{P_{avg}}}$$

is the well known Rayleigh-power PDF and P_{avg} is the average power of the Rayleigh distributed clutter, *n* is the collapsing factor and

$$F^{n-1}(x) = \int_0^x p(y)\,dy = 1 - e^{-\frac{x}{P_{avg}}} \tag{27}$$

The closed form solution of the PFA is available for the simple case where no integration of peak detected values occurs but becomes intractable when integration is introduced thereby necessitating the use of numerical or Monte Carlo techniques. Tasos and Haslam [14] examined the use of numerical convolution of the PDFs in equation 26 and compared it with the use of Monte Carlo methods. They showed that under most circumstance the Monte Carlo approach produces superior results. When the clutter PDF is generalized to a K-distribution, the application of the numerical convolution becomes impractical and it becomes necessary to solely employ Monte Carlo techniques to determine the detection performance. The effect of peak detection on the detection performance of a fast scanning radar is discussed by McDonald [15] in a report which presents Probability of Detection curves versus Signal to Clutter ratios for a variety of clutter conditions. The results can be used as a

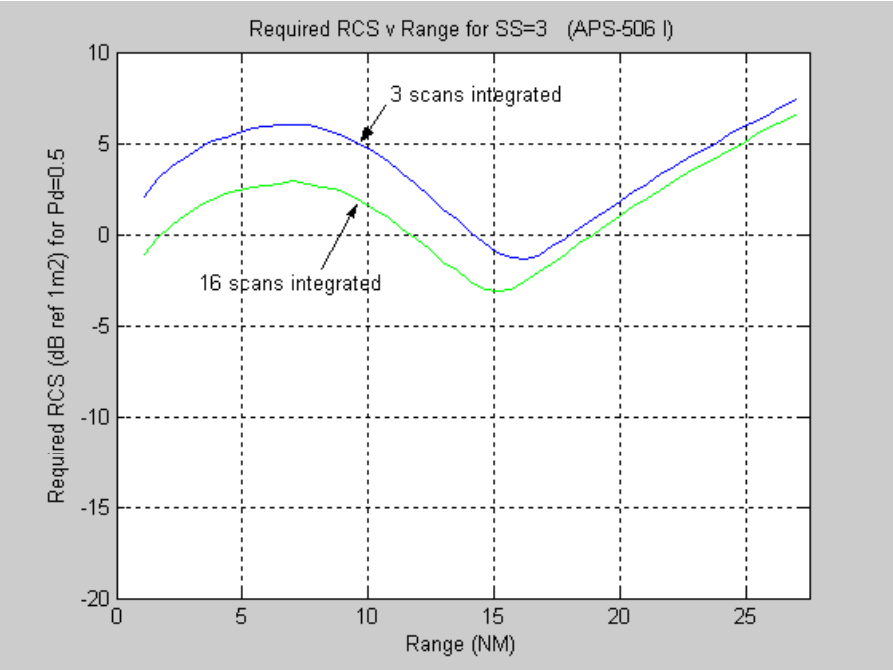

Figure 2. Required RCS for 50% probability of detection in Sea State 3 with assumption of integration of 3 and 16 independent scans.

rough guide for deducing collapsing loss factors under other radar configurations or the approach can be extended to generate specific results. Figure 4 presents an example of the effect of increased macrocell size on the required detection threshold for a spiky clutter (shape parameter ν=1) under a 10 scan binary integration.

2.3.6 Effects of Spatial Correlation of Clutter

In addition to the effects of temporal correlation within the clutter, it is also important to consider the effects of spatial correlation in the underlying clutter and, in particular, spatial correlation in the texture of the clutter. As discussed, cell averaging backgrounds (or some derivation thereof) are typically used to estimate underlying clutter power in a CUT so as to implement constant false alarm (CFAR) detection techniques.

For the case where the background length is small compared with the correlation length of the underlying clutter texture it is possible to get a good

estimate of the underlying clutter power within the CUT. As discussed above, the texture or clutter power varies as a result of the physical swell structure on the sea surface. This suggests that background sizes should be chosen to be much smaller then the length of the sea surface swell if one is to obtain a good local estimate. However, the improvements achieved by making the background smaller are limited by the fact that each measurement is a stochastic variable and from a statistical viewpoint, it is therefore necessary to use as many samples as possible to produce the most accurate background estimate.

The above case where a strong spatial structure is present can be contrasted with the case where little spatial correlation exists or the spatial scale is very short. Under conditions of small spatial correlation it is not possible to obtain a true localized estimate of background power and one is better off using the largest background size possible to obtain the best statistical estimate. Practically the maximum background size will be limited by considerations such as interference from other targets as well as non-homogeneity of clutter conditions.

In analogy with the discussion of temporal correlation, the cases in which the underlying scale of the spatial texture correlation are on the same order as the size of the background prove to be the most challenging. Currently no closed form solution exists and one is again forced to resort to Monte Carlo methods.

Fortunately, it is usually sufficient to consider only the cases where complete textural spatial correlation or no textural correlation exists when one is attempting to specify radar performance. Radar manufacturers will commonly employ multiple background estimator sizes (or allow the operator to adjust the background size) and utilise the estimates that best suit the underlying conditions. As a minimum, one local and one global background estimate are formed; the local background is typically quite small, on the order of 10's of samples while the global background are larger, on the order of 100's of samples. Under conditions of strong spatial correlation (relative to the extent of the background being employed) it is usually possible to get a sufficiently accurate estimate of the local background performance by using the CA-CFAR detection performance as given by equations 17 and 18 above. One caveat is that the logic used to choose the best background estimate will typically introduce an additional small loss factor that must be included in the calculations.

For the case of a global background, the assumption of constant texture across the background is violated and the actual performance is most accurately predicted using the fixed threshold detection performance equation 13. Where necessary these performances can be adjusted to allow for an additional loss

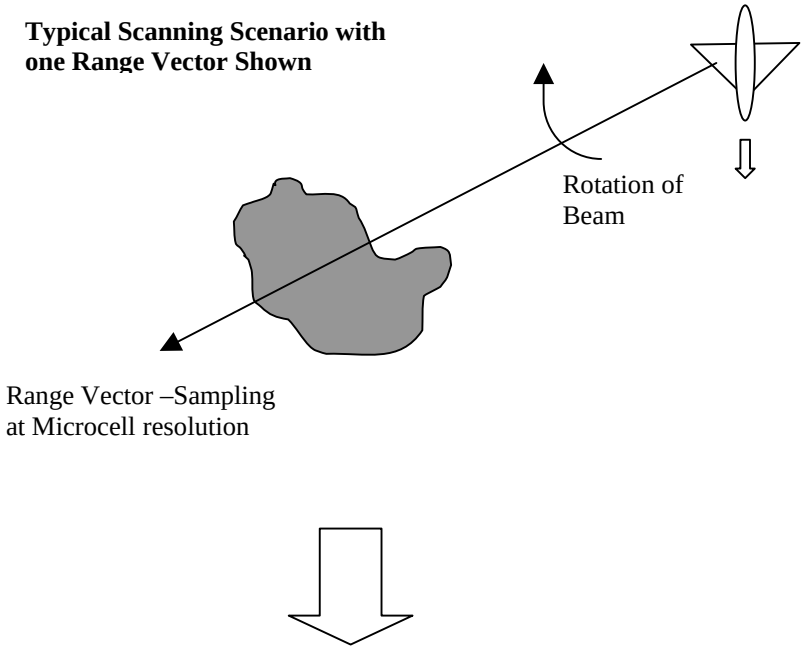

Figure 3. *Definition of microcell and macrocell.*

resulting from the finite size of the background (i.e. number of statistical samples). In practice the adjustment is typically small, Watt's [12] performed a Monte Carlo analysis which showed that the loss associated with using a 100

sample background window was only a fraction of a dB although the presence of correlation may increase this somewhat. In addition to this result Watt's used the Monte Carlo analysis to estimate the effect of exponentially decaying texture correlation of different scales on the prediction performance. While his numbers are strictly only applicable to this particular decay function they nevertheless prove useful as a guide to loss factors under other similar conditions.

2.3.7 Setting Detection Threshold

A correct setting of the detection threshold is critical to the operational effectiveness of the radar. Too low a setting will result in excessive false alarms which will either swamp the operator or overload the Track While Scan (TWS) function. Examination of equation 18 indicates that under condition of constant texture power across the background the correct threshold setting for a CA-CFAR is a simple function dependent on the number of background samples and the number of pulses integrated. Unfortunately these ideal conditions are almost never encountered in real operation and it becomes necessary to employ some sort of background characterization scheme to further refine the threshold setting.

Three approaches are commonly used to tackle the problem

1) Distribution Free (DF) detection
2) Measurement of characteristic parameters of an assumed PDF
3) Interpolation of threshold values

DF detection uses a ranking scheme to perform detection of targets. The rank of the CUT within the surrounding background is calculated and summed across the desired number of pulses before comparison to a detection threshold. The test is non-parametric if certain conditions are met, namely that the PDF is the same across all measurements within a given dwell and that all measurements are completely independent. The latter condition is the most difficult one to ensure in maritime conditions due to the underlying texture correlation present in sea clutter [16].

The second technique typically assumes a K-distribution and calculates the corresponding shape parameter and underlying power. The challenge with this approach is to find a sufficiently large and homogenous region to obtain enough points to accurately calculate the required parameters. In addition, a method must be derived to remove real persistent targets from the background region to avoid contaminating the parameter characterization; this becomes particularly important in target dense areas such as littoral regions. The actual underlying PDF must also be close to the assumed PDF if the derived threshold is to be accurate.

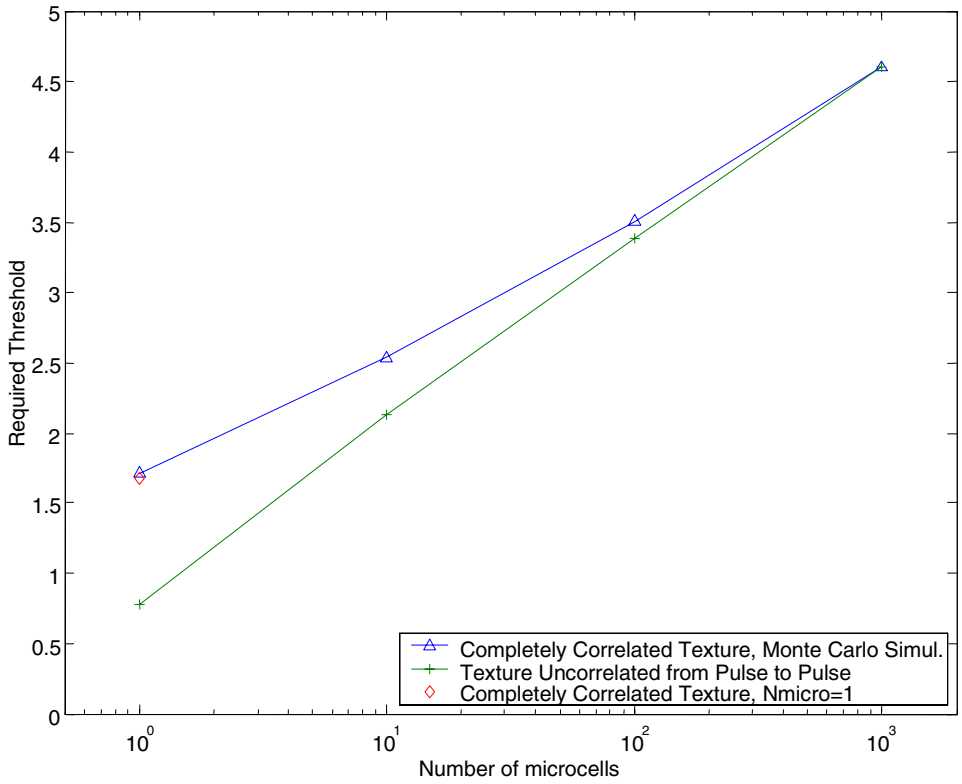

Figure 4. *Effect of macrocell size on threshold required to achieve $PFA_{n\text{-}macro}=10^{-4}$ under m out of n detection scheme (m/n=10/10) with ν=1. Green line shows analytically derived thresholds for case when clutter completely decorrelates from pulse to pulse. Blue line shows thresholds determined from Monte Carlo simulations when texture component of clutter remains completely correlated between integrated pulses. Diamond shows analytically derived threshold for case when texture component of clutter remains completely correlated between integrated pulses and macrocell length is equal to one microcell.*

Interpolation of threshold values is accomplished by testing a series of high PFA thresholds across a large background area which is assumed to be homogenous. The measured PFA versus threshold values are then extrapolated to obtain the required threshold corresponding to the desired operational PFA. Similar challenges in terms of homogeneity and target contamination exist as were encountered for the parameter estimation methods.

The techniques used to compensate for the inaccuracies in the threshold calculation are commonly empirical or ad hoc in nature and the details of their design are typically proprietary information unavailable to the radar purchaser. Because of this it is not possible to analytically model the effect of these

approaches on the overall detection performance and the evaluator must rely on loss factor characterizations provided by the manufacturer for a number of key operating conditions.

2.4 Specifying Radar Performance

One of the first and most critical steps in any radar procurement process is the preparation of the equipment specification. The preparation of the specification is a delicate balancing act in which the need to ensure that all the critical capabilities of radar performance are addressed in a verifiable way is balanced against the drawbacks of over-specifying the system. Over-specification of the requirements can unduly limit the flexibility of the manufacturer to modify their design to meet critical capabilities and, in addition, over-specification can lead to a large testing and verification burden (and associated expense) without resulting in any real added value or reliability to the final system.

The above sections discussed the various factors affecting detection performance modelling of radar systems and developed some of the mathematical tools and approximations necessary to perform this modelling. It is critical to keep in mind these modelling limitations during the preparation of the equipment specification; the limitations will guide the process as they reflect on our ability to compare competing radar systems and ultimately verify the performance of the delivered system.

Since radar systems will typically be fielded under a broad range of conditions and against varying targets it is extremely difficult, if not impossible, to comprehensively test radar systems prior to acceptance and, given the high cost of field testing, it becomes prohibitively expensive. As such it is necessary to verify system compliance using a mix of modelling, simulated environment testing and a limited selection of field tests.

Several decisions must be made as to how the clutter characteristics are set down in the specification. As discussed above, the AIMP and MHP procurement programs utilized K-distributed clutter models to describe the underlying clutter. The choice of a common clutter PDF is critical to ensuring that competing systems are being evaluated on equal terms. That said, an argument can be made that different systems could be optimized for different clutter models, each of which might be more applicable under specific conditions. For the purposes of the above procurements the K distribution was chosen as most representative of the broadest range of conditions under which the radar would operate. This conclusion was based on results within the published literature as well as past experience with clutter measurements collected by DRDC Ottawa. In addition, the widespread application of the K-

distribution in the literature ensured that all suppliers would be able to familiarize themselves with its application.

The choice of the clutter model is only the first step in the definition of the clutter parameters. As the above discussion on detection modelling highlighted, the spatial and temporal correlation of the underlying texture can have a significant impact on the performance of a radar system. Unfortunately under real conditions these parameters can vary widely and initial consideration would suggest that one assign a wide range of values to cover all conditions. However, this approach tends to impose an unnecessarily large burden of analysis and testing on the system and, in any case, it does not help much to narrow down the proposed systems as all will have their preferred region of operation.

It is often helpful when setting these parameters to consider what the architecture of the proposed systems will be, and what limitations exist in our ability to model the performance. This approach was taken during the development of the specifications for the procurements discussed in this report. For example, in the discussion above it was noted that cases where partial temporal correlation exists between the scans are difficult to model. If we know that the proposed systems all have scan rates of 60 rpm or less it will significantly simplify the analysis to specify that the texture of the clutter have a temporal correlation of 1s or less. This specification eases the modelling yet still ensures that the value is compliant with the general estimate of textural correlation being on the order of seconds. The issue of performance degradation due to the presence of longer texture correlation time in real conditions can then be more generally addressed by specifying additional functionality, such as additional scan rates. Similar reasoning can be applied to the specification of spatial correlation of the texture. The critical point that one would like to draw out is the radar's ability to exploit local texture knowledge when a strong underlying swell structure is present, and the ability to produce and use a large background global average when the correlation is not present. Therefore, one must specify at least two different correlation lengths which reflect these extremes. The application to intermediate lengths can again be addressed by specifying additional functionality such as adjustable background sizes or possibly an intermediate correlation length.

While the above approach to specification does not allow one to pin down all aspects of radar performance it has the important advantage of being mathematically tractable thereby ensuring that compliance with specifications can actually be confirmed with a reasonable degree of effort. This is particularly important during the early selection phase of a procurement as there may be many proposed radars and a detailed analysis cannot be

performed on all. The issue of testing and verification is discussed in more detail in the following section.

2.5 Testing and Verification of Radar Detection Performance

As discussed earlier, exhaustive field testing of all the radar performance specifications is difficult and cost prohibitive. In addition, field testing cannot be performed until well into the design cycle so there is a significantly higher risk impact from the identification of non-compliance at this late stage if field testing is used as the sole method of detection performance verification.

For the AIMP procurement a three stage detection performance verification approach has been used. The stages are as follows

1) modelling of radar detection performance

2) detection performance against simulated data

3) field trials.

The equipment specification contains a number of detection requirements for cases with different target types, detection ranges and sea states subject to the clutter detection model parameters discussed above. These specifications reflect the operational requirements of the radar with the caveat that practical design limitations are considered. Minimum and maximum detection ranges were specified for each case. A typical detection curve displays a near and far region in which PD drops to zero. Figure 5 represents a typical output of PD versus range for a Swerling 2 target from an altitude of 1000 feet. The near range falloff represents the effect of a degraded signal to clutter ratio i.e. the signal is clutter limited. The effect arises because of the steep incidence angle of the viewing geometry at near range which results in a very strong reflection from the sea surface. At far ranges the signal drops off due to the 4^{th} power dependence with range while the internal receiver noise is unaffected. This results in a falloff in the signal to noise ratio, i.e. the signal is noise limited.

During the first step of the verification process, all the operational cases are modelled. The anticipated Signal to Clutter plus Noise Ratio (SCNR) is used as the input to the detection algorithms developed above to determine the final detection probabilities. The SCNR is derived using the specified clutter models (GIT), equipment performance measurements (e.g. noise figure) and lumped loss or gain parameters to capture other factors affecting performance. To aid this type of work the calculation of SCNR and associated PD has been combined to produce the MaTaDOR detection model. Details of the model and

the calculation of SCNR are given in DRDC Technical Report TR 2001-159 [17].

While the modelling step enhances the confidence that the radar will meet detection specifications its accuracy depends on the success with which we were able to quantify the miscellaneous loss factors. Frequently there are signal processing steps, such as the introduction of edge detection techniques into the CA-CFAR scheme, for which the calculation of the loss factor is not mathematically tractable. In these cases it is often necessary to extrapolate using estimates of loss factors derived from field trials or from Monte Carlo modelling of the signal processor.

The second testing stage is designed to verify that the loss/gain factors that were used in the model are sufficiently accurate, i.e. that the approximations used in the models capture the behaviour of the actual signal processing chain. During this verification step, simulated K-distributed clutter is generated with embedded target signatures. This simulated data is then fed into the signal processor of the radar with a convenient injection point corresponding to the output of the Analog to Digital Converters (ADCs). A reduced subset of the original specification cases is tested, as the intent is not to verify that all specified detection cases are compliant but to verify that the earlier modelling step adequately represents the effects of the signal processing chain.

The final step represents the field testing of the systems. The radar will be installed on an airborne platform and flown against calibrated cooperative targets as well as targets of opportunity. Since airborne field tests must be planned and scheduled well in advance it is impossible to ensure that the environment conditions specified for each of the detection cases will exist during the trials. At this point the model developed for stage 1 and verified in step 2, can be used to extrapolate the detection results from the environmental conditions that actually occurred to the corresponding results for the conditions specified under the test cases. As an example, one can model with the verified loss and gain factors but input the actual measured clutter power and shape factor rather then using the GIT model and Watt's empirical formula for the shape parameter given above. This final step closes the loop on the verification cycle.

As discussed early, there can be larger variations between clutter returns predicted by the model and the actual clutter returns. In addition, other conditions such as atmospheric attenuation, shape parameter variation and ducting can have a significant impact on measured detection performance. Because of this uncertainly there is often significant pressure to reduce the specified detection performance to account for worst case conditions prior to

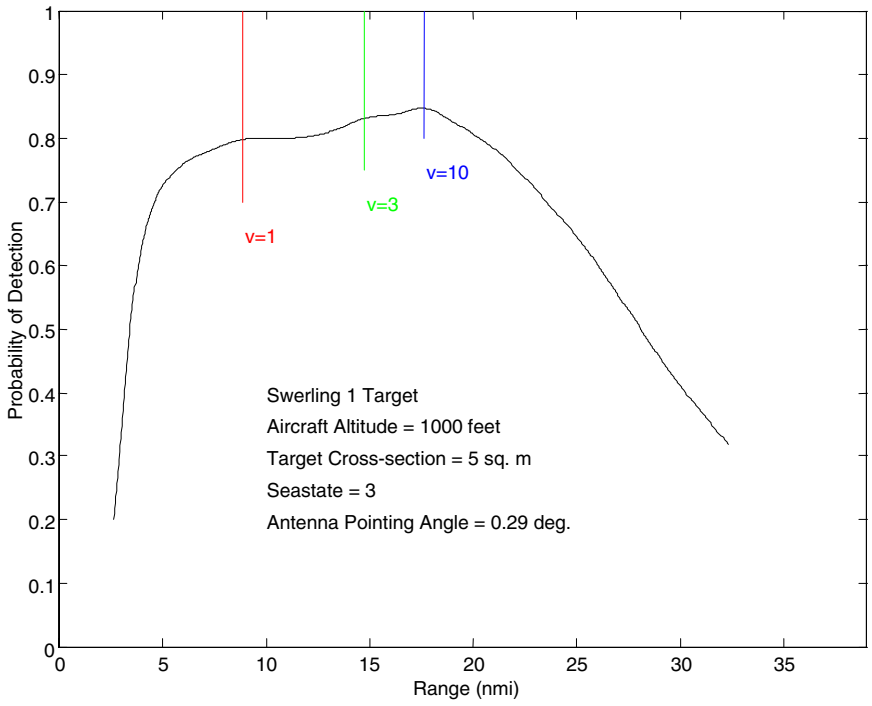

Figure 5. *Probability of detection versus range for 5 m^2 Swerling 1 target from aircraft altitude of 1000 feet with Douglas sea state 3. Range locations at which underlying K distribution shape parameter equals 1 (red), 3 (green) and 10 (blue) are indicated.*

testing so as to avoid non-compliant test items. This approach can lead to significant risks to the radar purchaser. One of the clear drawbacks is that a radar operating in conditions that are very close to the original modelled conditions will meet the specified test points even though its operation may be well below desired performance levels. Perhaps more subtle is the danger of missing performance holes. These performance holes occur when a radar produces excellent performance over a broad range of conditions but suffers from unexpected dropouts over a small range of conditions. An example would be a radar operating in a high resolution mode which is correctly detecting most existing targets but is missing some of the extremely large targets due to leakage of target returns into the cell averaging background. If the specified detection performance has been set too low this radar may meet the requirements of the test plan even though it is clear that a design deficiency is present. It is important to recognize these risks and maintain specifications at a sufficiently highly level so as to ensure that such deficiencies can be captured and addressed. The downside of this approach is that additional paperwork in

the form of waivers or deviations will be required to deal with the potentially larger number of non-compliant test items that may result.

It is critical to perform the field testing as early as possible in the procurement process, and certainly well before delivery and installation begins on the target aircraft. For the AIMP an incremental testing program was designed to test functionality and relieve risk factors. A series of test flights will be performed on the manufacturer's test aircraft against cooperative targets and targets of opportunity to exercise the functionality of the various modes. The series of tests will be applied against different operating modes as the development is completed for each mode. Indeed, the final complete radar system will not be available until some point later in the process but older, established modes will be tested at this earlier stage for acceptance by DND and the prime contractor. This approach will ensure that the work load associated with demonstrating compliance will be spread out more evenly and that risk is retired at the earliest possible stage.

3. Evaluation of Synthetic Aperture Radars

The criteria for characterizing the performance of a synthetic aperture radar can generally be divided into three areas: the dynamic range of the radar, the sensitivity of the complete system or its noise-equivalent-sigma-zero (σo_{NE}), and the details of the final system impulse response in both range and cross-range. Dynamic range and σo_{NE} are derived from measurements and models. Impulse response characterization, or image quality, can be predicted by analysis or simulation but requires extensive modelling of the radar signal characteristics throughout the complete transmit, receive and processing chains. Therefore, we discuss impulse response characterization in a more straightforward manner, through measurements on real imagery which contains known corner reflectors.

3.1 Dynamic Range

3.1.1 Instantaneous Dynamic Range

The dynamic range of a radar represents the range of signal levels that it can measure. It is the power ratio of the largest to the smallest signals that the system can sample. For a radar employing an eight bit analog-to-digital (A/D) converter, where one bit is reserved as the sign bit, the magnitudes of the signals it can sample range from 1 to (2^7-1). The dynamic range corresponding to these signal power levels is therefore $20 \times \log_{10}((2^7-1)/1) = 42$ dB. A rule of thumb is that each bit supplies 6 dB of dynamic range. In practice, this full dynamic range is not available due to the fact that the power level of the receiver noise floor occupies the lower bits. The A/D converters are typically calibrated such that minimally the first bit is triggered by receiver noise. In this case the instantaneous dynamic range which can be sampled by the A/D converter is therefore 36 dB relative to receiver noise.

This a priori knowledge of the limitation of the dynamic range of the A/D converter is used in the design of a limiting amplification stage which immediately precedes the A/D. It is this stage of the receiver which saturates when signals exceeding the expected dynamic range are received. Saturation is undesirable as it carries through to nearby signals as well as introducing amplitude and phase distortions into them. Synthetic aperture radar is a coherent process, therefore these distortions will be manifested in the image beyond the actual region from which the saturating signal originated. Subsequent to A/D conversion is the compression in range and the compression in azimuth. Both of these processes typically add 30 to 40 dB of dynamic range to the signal. Therefore, the resulting dynamic range can exceed 100 dB.

3.1.2 Spurious Free Dynamic Range

In a coherent radar system, when a pair of sinusoidal signals are applied to the input of a receiver they mix in the RF stages and create intermodulation products. When these intermodulation products are within bandwidth and of sufficient strength, the receiver treats them as real incoming signals and downconverts them to IF.

The resulting intermodulation products are referred to as spurious signals. Spurious Free Dynamic Range (SFDR) is the power level by which a signal, which has been generated as an intermodulation product, must be lower than the originating signal. It is the second-order and third-order spurious signals which are of concern. Given two strong signals both within the receiver passband and of frequency f_1 and f_2, the second order intermodulation distortion will appear at frequencies f_1-f_2 and f_2-f_1. Similarly, the third order intermodulation distortion will appear at frequencies $2f_1$-f_2 and f_1-$2f_2$. Again, when these products fall within the receiver passband, they are seen as valid signals in the subsequent downconversion and processing. The receiver must be designed to achieve a certain desired level of SFDR. For a fine resolution imaging SAR this is typically greater than 40 dB. Proper receiver design is important as spurious signals receive the same amount of pulse compression gain and azimuth compression gain as real signals, and will thus show up as sidelobes and false targets in the radar image.

3.2 Noise-Equivalent-Sigma-Zero

Noise-equivalent-sigma-zero (σo_{NE}) is a measure of the sensitivity of the imaging radar against spatially distributed noise. It is the smallest distributed clutter that can be seen in the presence of receiver noise. In general, this performance metric specifies the minimum signal to receiver noise ratio that can be obtained for a given terrain reflectivity (it is equivalent to the noise return from the radar resolution cell). Within the following, noise introduced by range ambiguities are not considered.

The maximum radar range is the distance beyond which the target cannot be detected. It occurs when the received echo signal power just equals the minimum detectable signal. Using this premise and starting from the simple form of the radar range equation [1], the noise-equivalent-sigma-zero can be derived as:

$$\sigma o_{NE} = \frac{kB_{rec}T}{G_{azimuth}G_{range}P_r}, \tag{28}$$

where

P_r is the power received from a single transmitted pulse,

$G_{azimuth}$ is the compression gain in azimuth,

G_{range} is the compression gain in range,

k is Boltzmann's constant,

B_{rec} is the receiver bandwidth in Hz,

P_r is the power received from a single transmitted pulse and

T represents the thermal noise power generated by a receiver of bandwidth B_{rec}. P_r is further defined as

$$P_r = \frac{P_t(G_\vartheta \lambda)^2 \rho_{azimuth}\rho_{range}}{(4\pi)^3 R^4 L_{fixed}(L_{atmospheric}R/1000)} \tag{29}$$

where G_θ is the antenna gain in azimuth,

λ is the transmitted signal wavelength,

P_t is the transmitted power,

$\rho_{azimuth}$ is the resolution in azimuth after synthetic aperture processing,

ρ_{range} is the resolution in range after pulse compression,

R is the range to the target,

L_{fixed} is a lumped element constituting the sum of all of the fixed losses (L_t=transmission loss, L_r=receive line loss, L_w=signal processing window loss, L_{rad}=two-way radome loss and $L_{antenna}$=azimuth beamshape loss) and

$L_{atmospheric}$ is a range dependent attenuation loss. $G_{azimuth}$ is defined as

$$G_{azimuth} = \frac{\lambda R \cdot PRF}{2V_{ac}\rho_{azimuth}} \tag{30}$$

where *PRF* is the radar pulse repetition frequency, and V_{ac} is the ground speed of the aircraft. G_{range} is defined as

$$G_{range} = B_t \tau_{pulse} \tag{31}$$

where B_t is the bandwidth of the transmitted pulse and τ_{pulse} is the width of the transmitted pulse. Using the above formula it can be seen that sensitivity increases (i.e. becomes more negative) if P_t increases, λ increases, G_θ increases, τ_{pulse} increases, R decreases, B_{rec} decreases and T decreases. Table 1 lists typical values for computation of σo_{NE}. Figure 6 plots σo_{NE} versus slant range for ρ_{range}=$\rho_{azimuth}$=1.0 m, 5.0 m and 10.0 m. In these plots the performance at each range point is computed assuming the maximum gain in elevation. In practice, for a fixed swath centre range the performance would vary across the swath as a function of the gain of the elevation beampattern.

Noise-equivalent-sigma-zero is used for stripmap and landspot imaging. For the same pixel resolution, the σo_{NE} of a stripmap imaging system is the same as that of a landspot imaging system. Performance varies across the imaged swath as a function of the gain of the elevation beam. It can be seen that the system sensitivity varies with resolution and range, being most sensitive at near range. Sigma zero (σo) is a function of terrain type, aircraft altitude and imaging range. At 20 nm, σo can range from –30 dB for flat, smooth terrain to –15 dB for mountainous terrain. Similarly, at 20 nm, the σo_{NE} can range from –58 dB for a SAR with 10 m resolution to –48 dB for a SAR with 1 m resolution. Table 2 describes the resulting SNRs . Good image quality typically requires signal-to-noise ratios of 10 dB. The margins for system performance based on this assumption are also given in Table 2. It can be seen that for this set of parameters and an expectation of a minimum SNR of 10 dB, the low resolution modes have ample margins to allow imaging in a broad range of terrain types.

However, for the high resolution SAR modes, the margin becomes very small for low reflectivity terrain.

In the case of Seaspot imaging we do not employ noise-equivalent-sigma-zero as the performance metric. Rather, we examine the conventional signal-to-noise-ratio as we are interested in the smallest detectable scatterer cross-

section. This is because noise-equivalent-sigma-zero is relevant to targets where the radar cross-section is assumed to be uniformly distributed across the resulting image pixel. In the Seaspot mode, where the target is a ship on the open ocean, the fine resolution target image is a collection of pixels, each of which is generally dominated by a different point scatterer. The total radar cross-section of the target is derived from multiple scatterers distributed in range and cross-range about the target. In summary, of interest is the SNR for

a given point scatterer radar cross-section as a function of range for various antenna beam depression angles.

Table 2: Typical parameters for noise-equivalent-sigma-zero calculations based on DRDC Ottawa XWEAR data acquisition system.

Parameter	Quantity
B_{rec}	900 MHz
T	600 K
k	1.38e-23
P_t	50 kW
G_θ	20 dB
λ	0.0307 m
ρ_{range}	Variable
$\rho_{azimuth}$	Variable
R	Variable
L_{fixed}	5.5 dB (L_t=0.9, L_r=0.6, L_{window}=0.5, L_{rad}=1.9, $L_{antenna}$=1.6)
$L_{atmospheric}$	0.011 dB/km
PRF	800
V_{ac}	150
B_t	800 MHz
τ_{pulse}	5 us

Table 3: Noise-equivalent-sigma-zero and expected imaging performance.

Terrain Type	σo (dB)	σo_{NE} (dB) (res.=10 m)	SNR (dB)	Margin (dB) (assumes 10 dB min SNR)	σo_{NE} (dB) (res.=1 m)	SNR (dB)	Margin (dB) (assumes 10 dB min SNR)
Flat	-30	-58	28	18	-48	18	8
Mountains	-15	-58	43	33	-48	33	23

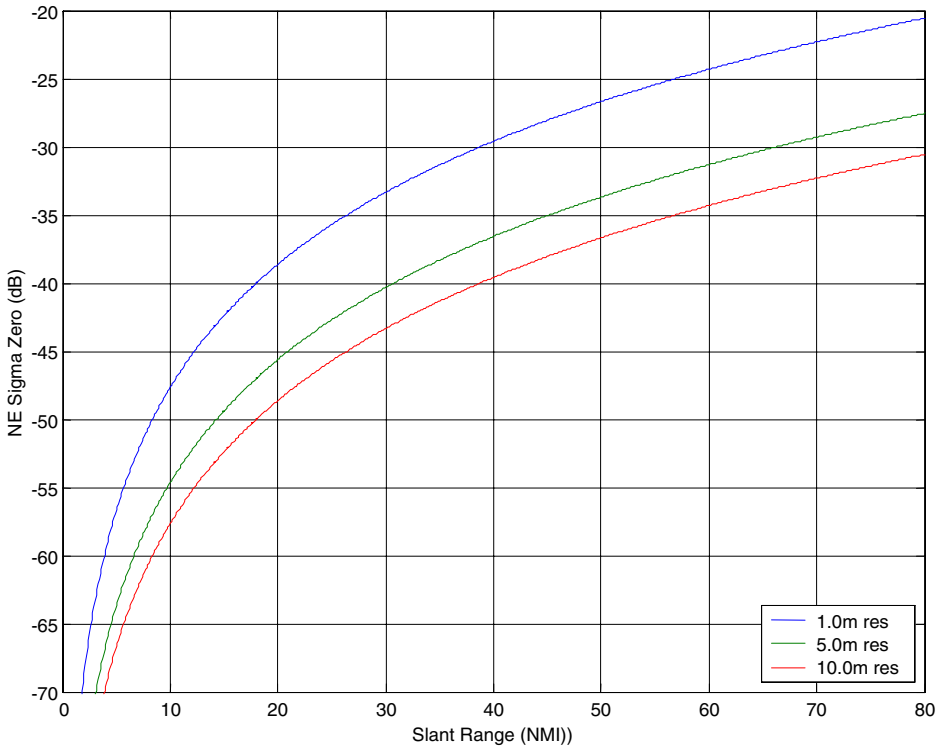

Figure 6. *σo_{NE} versus slant range.*

3.3 Impulse Response Characterization

The impulse response of a synthetic aperture radar can be characterized in either the range direction (response is a product of pulse compression) or the azimuth direction (response is a product of synthetic aperture compression). The parameters typically used to characterize the impulse response are resolution, ISLR (integrated sidelobe ratio), and PSLR (peak sidelobe ratio). For the purposes of calculating these quantities, the regions of the impulse response are first defined as follows:

Mainlobe region: the region centred on the point midway between the –3 dB points of the main peak and having a width equal to 3x the –3 dB width of the mainlobe peak.

Near region: the region extending from the edges of the mainlobe region (i.e. 1.5x the –3 dB width from the centre of the mainlobe region) out to 10x the –3

dB width from the centre of the mainlobe region on either side of the mainlobe. The value of 10x can be increased if appreciable energy is expected beyond this region.

Far region: on either side of the mainlobe, the region extending from 4x the –3 dB width from the centre of the mainlobe region out to; i) the transmitted pulse length in range in the case of range impulse response, ii) the synthetic aperture length in azimuth in the case of cross-range impulse response. For practical regions the actual extent of the Far region used in the measurement of the impulse response is less than the pulse or synthetic aperture length to avoid introduction of interfering target impulse responses and loss of information due to the edges of the imagery.

The impulse response characteristics can now be defined as:

Resolution: the width of the impulse response measured at the –3 dB level.

ISLR (Integrated sidelobe ratio): the ratio of the energy within the Near region to the energy within the Mainlobe region.

$PSLR_{Near}$: the peak sidelobe level within the Near region compared to the level of the peak of the mainlobe. This measurement captures most of the low-order phase error effects which have not been compensated for by the motion compensation system or autofocus.

$PSLR_{Far}$: the peak sidelobe level within the Far region compared to level of the peak of the mainlobe.

Figure 7 is an example of an impulse response (pulse compression or synthetic aperture compression). Within this figure the Far Region is limited to 10x the –3dB width on either side of the centre of the mainlobe.

For the land imaging modes, stripmap and landspot, the impulse responses are deterministically computed (outside of autofocus in the azimuth direction). Thus, for these modes, the impulse response measurements are applicable in both the range and azimuth directions. For seaspot, the impulse response measurements are only applicable in the range direction as the impulse response in azimuth (Doppler) is computed adaptively.

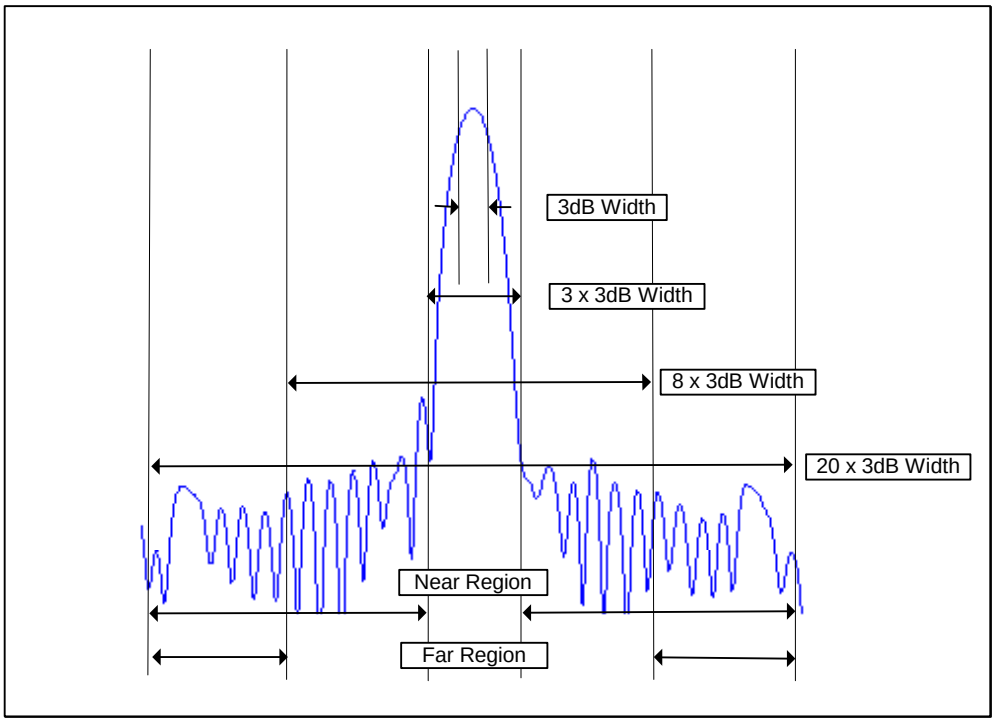

Figure 7. Impulse response: Near and far region specifications.

4. Conclusions

This report documented work performed over a multiyear period in support of the radar procurements for AIMP and MHP. The report focused on one aspect of the evaluation process, namely the specification and modelling of the maritime surveillance and SAR modes.

The choice of appropriate models for sea clutter and target behaviour was discussed along with the limitations and tractability of the detection performance solutions. Useful simplifications and approximations were presented with appropriate cross-references to supporting documentation.

The coupled issues surrounding the preparation of a requirements specification, and the supporting test and verification plan were discussed. The philosophies employed in the development of the specification and testing plans are highly dependent on the modelling limitations discussed above and examples were given of how the requirements are tailored to complement the modelling.

The second section of the report dealt with the performance of a surveillance radar operating in synthetic aperture modes. The system level performance of a SAR was looked at from three different viewpoints. First of all, the dynamic range of the radar in its' receive mode was discussed. Secondly, the actual imaging sensitivity of the radar was quantified and finally, the imaging performance of the radar is summed up by examination of the output image quality through characterization of the impulse response of the radar.

5. References

1. Skolnik M. : *Introduction to Radar Systems*, McGraw-Hill Book Company, Toronto, 1980.

2. Ward, K.D. : 'A radar sea clutter model and its application to performance assessment', *IEE Conf. Publ. 216 (Radar '82)*, 1982, pp.203-207.

3. Ward, K.D. and Watts, S.: 'Radar sea clutter', *Microwave J.*, June 1985, 28, pp. 109-121.

4. Watts, S.: 'Radar detection prediction in K-distributed sea clutter and thermal noise', *IEEE Trans. AES*, 1987, **23**, pp.40-45.

5. Horst, M.M., Dyer, F.B. and Tuley, M.T.: "Radar Sea Clutter Model", *URSI Digest, Int. IEEE AP/S URSI Symp.*, pp.6-10, 1978.

6. Watts, S and Wicks, D.C.: 'Empirical Models for Detection Prediction in K-distribution Radar Sea Clutter', *IEEE International Radar Conference*, pp.189-194, 1990.

7. Watts, S.: 'A Practical Approach to the Prediction and Assessment of Radar Performance in Sea Clutter', *IEEE International Radar Conference*, pp.181-186, 1995.

8. Skolnik, M.: *Radar Handbook*, McGraw-Hill Book Company, Toronto, 1990.

9. Hou, X. and Morinaga, N.: 'Detection Performance in K-Distributed and Correlated Rayleigh Clutters', *IEEE Tran.s AES*, 1989, **25**, pp. 634-641.

10. Oliver, C.J.: 'Optimum texture estimators for SAR clutter', J. Phys. D: Appl. Phys., 1993, 26, pp.1824-1835.

11. Dillard, G.M.: 'Binary Detection of Randomly Occurring Signals', *Naval Electronic Laboratory Center Research and Development Report*, 1976.

12. Watts, S.: 'Cell averaging CFAR gain in spatially correlated K-distributed clutter', *IEEE Proc.-Radar, Sonar, Navig.*, 1996, **143**, pp. 321-327.

13. Papoulis, A.: *Probability, Random Variables, and Stochastic Processes*, McGraw-Hill Book Company, Toronto, 1984

14. Drosopoulous, A. and Haslam, G., ‘Peak Detection of Swerling Type Targets Part 1: Detection Probabilities in White Noise’, *DREO R 1193*, 1985. Defence Research Establishment Ottawa

15. McDonald, M., ‘Peak Detection in Simulated K-Distributed Clutter’, *DREO TR 2001-144*, 2001. Defence Research Establishment Ottawa

16. Watts, S.: ‘Radar Clutter and CFAR Detection’, *Radar 2004 Tutorial*, 2004.

17. McDonald, M.: ‘Maritime Target Detection Operating Range (MaTaDOR) Simulation Program’, *DRDC Ottawa TR 2001-159, 2001*. Defence R&D Canada - Ottawa

DOCUMENT CONTROL DATA

(Security classification of title, body of abstract and indexing annotation must be entered when the overall document is classified)

1. ORIGINATOR (the name and address of the organization preparing the document. Organizations for whom the document was prepared, e.g. Establishment sponsoring a contractor's report, or tasking agency, are entered in section 8.)

DEFENCE R&D CANADA – OTTAWA
DEPARTMENT OF NATIONAL DEFENCE
OTTAWA ONTARIO CANADA K1A 0K2

2. SECURITY CLASSIFICATION (overall security classification of the document, including special warning terms if applicable)

UNCLASSIFIED

3. TITLE (the complete document title as indicated on the title page. Its classification should be indicated by the appropriate abbreviation (S,C or U) in parentheses after the title.)

Specification and Modelling of Maritime Surveillance and SAR Performance for Procurements (U)

4. AUTHORS (Last name, first name, middle initial)

MC DONALD, MICHAEL K.; DAMINI, ANTHONY

5. DATE OF PUBLICATION (month and year of publication of document)	6a. NO. OF PAGES (total containing information. Include Annexes, Appendices, etc.)	6b. NO. OF REFS (total cited in document)
November 2004	39	17

7. DESCRIPTIVE NOTES (the category of the document, e.g. technical report, technical note or memorandum. If appropriate, enter the type of report, e.g. interim, progress, summary, annual or final. Give the inclusive dates when a specific reporting period is covered.)

DRDC TECHNICAL REPORT

8. SPONSORING ACTIVITY (the name of the department project office or laboratory sponsoring the research and development. Include the address.)

DEFENCE R&D CANADA – OTTAWA
DEPARTMENT OF NATIONAL DEFENCE
OTTAWA, ONTARIO, CANADA, K1A 0K2

9a. PROJECT OR GRANT NO. (if appropriate, the applicable research and development project or grant number under which the document was written. Please specify whether project or grant)	9b. CONTRACT NO. (if appropriate, the applicable number under which the document was written)
3DT02	

10a. ORIGINATOR'S DOCUMENT NUMBER (the official document number by which the document is identified by the originating activity. This number must be unique to this document.)	10b. OTHER DOCUMENT NOS. (Any other numbers which may be assigned this document either by the originator or by the sponsor)
DRDC Ottawa TR 2004-238	

11. DOCUMENT AVAILABILITY (any limitations on further dissemination of the document, other than those imposed by security classification)

(X) Unlimited distribution
( ) Distribution limited to defence departments and defence contractors; further distribution only as approved
( ) Distribution limited to defence departments and Canadian defence contractors; further distribution only as approved
( ) Distribution limited to government departments and agencies; further distribution only as approved
( ) Distribution limited to defence departments; further distribution only as approved
( ) Other (please specify):

12. DOCUMENT ANNOUNCEMENT (any limitation to the bibliographic announcement of this document. This will normally correspond to the Document Availability (11). However, where further distribution (beyond the audience specified in 11) is possible, a wider announcement audience may be selected.)

Unlimited

13. ABSTRACT (a brief and factual summary of the document. It may also appear elsewhere in the body of the document itself. It is highly desirable that the abstract of classified documents be unclassified. Each paragraph of the abstract shall begin with an indication of the security classification of the information in the paragraph (unless the document itself is unclassified) represented as (S), (C), or (U). It is not necessary to include here abstracts in both official languages unless the text is bilingual).

The work performed in support of the radar procurements for the Aurora Incremental Modernization Program (AIMP) and the Maritime Helicopter Program (MHP) during the evaluation and design phases is presented. The report focuses on the maritime surveillance and Synthetic Aperture Radar (SAR) modes and develops appropriate methods for predicting and modelling their respective performance. Issues such as the choice of appropriate target and clutter models, detection techniques and SAR imaging performance are described along with an analysis of the modelling limitations and cross-references to supporting documentation. The coupled issues surrounding the development of the requirements specification and the supporting test and verification plan are also discussed. The philosophies employed in the development of specifications and test plans, and the dependencies on the modelling limitations are presented and examples provided of how the requirements are tailored to complement the modelling techniques. A discussion of potential pitfalls in specification and testing approaches is provided along with examples.

14. KEYWORDS, DESCRIPTORS or IDENTIFIERS (technically meaningful terms or short phrases that characterize a document and could be helpful in cataloguing the document. They should be selected so that no security classification is required. Identifiers such as equipment model designation, trade name, military project code name, geographic location may also be included. If possible keywords should be selected from a published thesaurus. e.g. Thesaurus of Engineering and Scientific Terms (TEST) and that thesaurus-identified. If it is not possible to select indexing terms which are Unclassified, the classification of each should be indicated as with the title.)

MARITIME SURVEILLANCE
RADAR
SAR

Defence R&D Canada

Canada's leader in defence
and national security R&D

R & D pour la défense Canada

Chef de file au Canada en R & D
pour la défense et la sécurité nationale

www.drdc-rddc.gc.ca